LETTER

Polymer-Templated Nanospider TiO_2 Thin Films for Efficient Photoelectrochemical Water Splitting

Honghan Fei,[†] Yuchen Yang,[†] David L. Rogow,[†] Xiaojuan Fan,[†,‡] and Scott R. J. Oliver*[,†]

Department of Chemistry and Biochemistry, University of California, Santa Cruz, 1156 High Street, Santa Cruz, California 95064, and Department of Physics, Marshall University, One John Marshall Drive, Huntington, West Virginia 25755

ABSTRACT We have discovered a facile and inexpensive approach to fabricate "nanospider" TiO_2 thin films with not only an amazing morphology but highly efficient water splitting to produce hydrogen. Our method employs benzene-swollen poly(ethylene glycol) as a sacrificial organic polymer to template the semiconductor thin film. The synthesized TiO_2 thin films are highly crystalline with optimized particle and channel size to enhance the liquid-semiconductor junction interaction. This enhanced contact area leads to more than twice the water splitting performance than conventional P25 thin films. In addition, the nanospider thin films also outperform P25 films in the photodegradation of toxic organics.

KEYWORDS: photoelectrochemical cells • water splitting • TiO_2 thin film • polymer templating • alternative energy

INTRODUCTION

TiO_2 is a wide band gap semiconductor attracting much attention since the discovery of Gratzel type dye-sensitized solar cells and the Honda-Fujishima effect of photoelectrochemical (PEC) cells (1, 2). Various nanostructures based on TiO_2 and their properties have been studied in detail, including nanowires (3), nanotubes (4), nanorods (5, 6), nanodisks (6), nanoflowers (7) and nanotrees (8). Considering the extreme environmental need for clean energy systems, recent effort has focused on using these nanomaterials for water splitting to produce hydrogen as well as the photodegradation of toxic organic dyes (7, 8).

The use of H_2 as an efficient and environmentally clean energy carrier is an essential part of future energy production. A clean source of H_2 is also required if CO_2 recycling is to be realized (9, 10). Semiconductor/liquid junction PEC cells are an emerging solar energy conversion system to produce hydrogen. They often utilize TiO_2 as photocatalyst, which is nontoxic, low-cost, and biocompatible (2). This configuration is capable of continuously producing H_2 based on water splitting, $2H_2O + h\nu \rightarrow 2H_2 + O_2$, as long as the cell is illuminated. With the discovery of various nanomorphologies of TiO_2 (11−14), the light-to-hydrogen efficiency has been effectively advanced over bulk titania. Despite the low-cost, convenient synthesis, high crystallinity, small particle size, and large semiconductor-liquid contact area, TiO_2 or ZnO photoelectrode PECs for water splitting are still limited because of low overall light-to-hydrogen conversion efficiency, typically 0.15% or lower (14−16).

Polymer templating of porous metal oxides is a well-established method and has been used to template ordered/quasi-ordered/disordered mesoporous metal oxides (17). Our group and others (most notably, Caruso and co-workers) have used ethanol and/or water solvated polymers to obtain porous metal oxides, because of the evaporation of the solvent and/or thermal decomposition of the polymer template (18−22). Meanwhile, we have also investigated organic solvent swollen polymers, with promising performance as dye-sensitized solar cells (23, 24).

Herein, we report a convenient and low-cost method to synthesize highly-crystalline TiO_2 thin films displaying a "nanospider" morphology over the entire substrate. The method utilizes benzene-swollen polyethylene glycol (PEG) as a structure-directing template to support the nanospider growth, and the unprecedented nanochannel morphology greatly increases contact with a surrounding solvent. The films show over double the photocatalytic performance compared to P25 type films, for both PEC water splitting and organic dye degradation.

EXPERIMENTAL SECTION

Preparation of the TiO_2 Nanospider Thin Film. Five weight percent polyethylene glycol (Alfa Aesar) was stirred and dissolved in 10 mL of benzene (Aldrich), followed by titanium isopropoxide (Acros Organic). The viscous mixture was stirred mechanically in a closed vial for 3 h. The resultant transparent solution was spin-coated at 1000 rpm for 30 s on F-doped SnO_2 (FTO) glass (Hartford Glass Co.). The FTO had been precleaned with ethanol and deionized water under sonication, followed by drying under an N_2 stream, and edge area defined by applying tape. The thin film was heated in a tube furnace at a rate of 2 °C/min to the desired annealing temperature and soaked for 2 h. The P25 thin film was deposited by spin-coating

* Corresponding author. E-mail: soliver@chemistry.ucsc.edu.
Received for review February 1, 2010 and accepted March 26, 2010
† University of California, Santa Cruz.
‡ Marshall University.
DOI: 10.1021/am100087b

Published on Web 04/05/2010

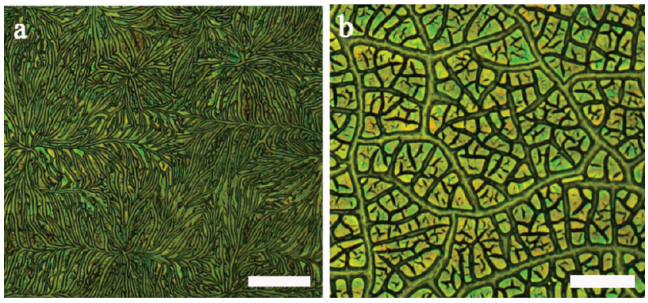

FIGURE 1. Optical micrograph of (a) the TiO_2 nanospider morphology synthesized from 5 wt % PEG; (b) TiO_2 morphology synthesized from 6 wt % PEG (scale bars 50 μm).

the P25 paste in ethanol on FTO glass and then heated in an oven set to 110 °C. For the P25 thin film only, the procedure of spin-coating was repeated until the film thickness was ca. 1 μm [monitored by cross-section scanning electron microscopy (SEM)]. The 15 nm nanoparticle thin film was grown by hydrolysis of titanium n-butoxide under acidic medium (diluted HNO_3 with pH 1.2). The deposition procedure was the same as for P25, then the film was annealed at 450 °C for 2 h.

Photoelectrochemical Measurements. The nanospider thin film anode was prepared by connecting a copper wire to a bare portion of the FTO glass after tape removal and secured with high-purity silver conducting paint (Alfa Aesar). The cell was then sealed on all edges with epoxy resin except for a working electrode surface area of ~0.10 cm^2. An electrolyte solution of 0.1 M NaOH and an Ag/AgCl reference electrode (+0.198 V vs NHE) was employed, along with a coiled Pt wire counter electrode during all testing. All PEC measurements were carried out on a Solartron 1280B Workstation coupled to an infrared water-filled filter (Oriel no. 6127), aligned in a monochromator (Oriel Cornerstone 130 1/8 m). A 1000 W Xe lamp was utilized as a white-light source and irradiance was measured with a power meter.

Methylene Blue (MB) Degradation Photocatalysis. A 6W compact UV lamp (UVL-56, UVP Inc., intensity 1.35 mW/cm^2 at 365 nm) was used as the light source, with the sample holder placed on its side to maximize exposure. For a typical experiment, a TiO_2 thin film was suspended in the MB solution for 10 min under dark conditions to achieve absorption equilibrium before carrying out the photocatalysis reaction. A UV−vis spectrometer (model 8452A, Hewlett-Packard) was used to determine the concentration of MB solution versus UV exposure time.

RESULTS AND DISCUSSION

A nonpolar organic solvent is required during the deposition; attempts to carry out the reaction in ethanol, dichloromethane, or acetonitrile were unsuccessful. Stirring in a closed environment to avoid overly rapid hydrolysis of the TiO_2 precursor is also essential to reach a homogeneous morphology. The substrate has no impact on forming the nanospider: the thin film can be grown on bare glass, F-doped tin oxide (FTO) glass, indium tin oxide (ITO) coated glass, or bare silicon wafer.

Top-view optical (Figure 1) and SEM (Figure 2a,b) micrographs of as-prepared TiO_2 nanospider thin films show a homogeneous morphology of interconnected nanochannels over the entire surface (2 cm ×2 cm). These nanochannels are all of similar ~1 μm width and define ca. 20% the area of the film; the remaining area is raised domains of TiO_2. Cross-sectional SEM images (Figure 2c and Figure S1 in the Supporting Information) of the TiO_2 nanospider on FTO glass show that the nanochannels are defined by the TiO_2 coated area, with a depth of around 1.2 μm. Slightly increasing the PEG ratio from 5 to 6 wt % greatly changed the thin film morphology by increasing the nanochannel width, reducing the titania coverage on the substrate (Figures 1 and S1).

Irregular or discontinuous cracks usually lead to less coverage of titania on the substrate, and in turn reduced light absorption and photocatalytic performance. In our case, however, the presence of controlled narrow-width channels leads to larger semiconductor-liquid contact area at the channel walls as well as small cracks in the island regions (Figure 2b,c). We are thus balancing these two effects of larger semiconductor-liquid contact (via channels and island cracks) while maximizing TiO_2 coverage. Considering the greater homogeneity and semiconductor coverage of the thin film synthesized from 5 wt % PEG over 6 wt % PEG (Figure 1), we employed the former for photocatalytic investigation.

A possible formation mechanism for this nanostructure is self-assembled phase separation of the solvent-swollen PEG and titania precursor. PEG is a hydrophilic long-chain polymer, whereas titanium(IV) isopropoxide [$Ti(O^iPr)_4$] is a hydrophobic titanium precursor with bulky organic side chains surrounding the metal centers. Hydrophilicity/hydrophobicity could lead to phase separation of the PEG and $Ti(O^iPr)_4$. In addition, $Ti(O^iPr)_4$ hydrolyzes more rapidly than titanium(IV) n-butoxide [$Ti(O^nBu)_4$] and titanium(IV) n-propoxide [$Ti(O^nPr)_4$] (25). This observation

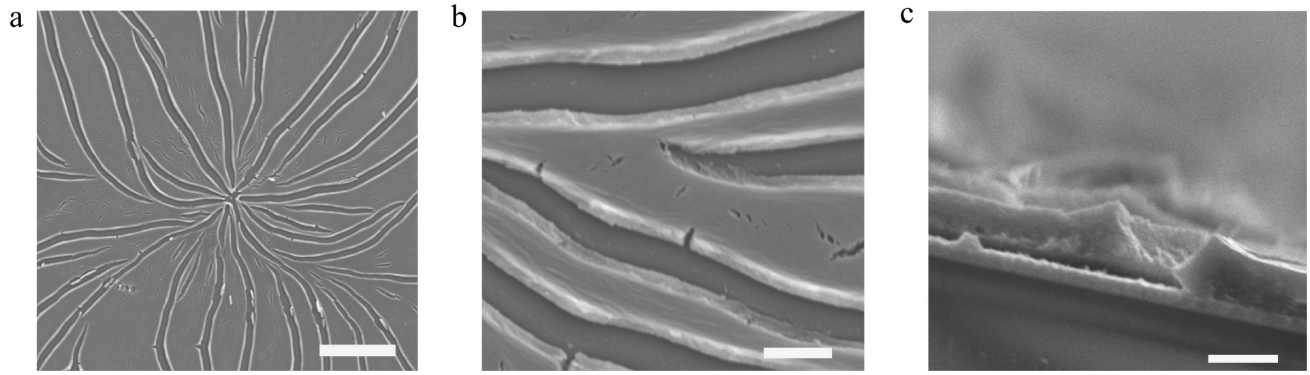

FIGURE 2. (a, b) Top-view SEM images of the TiO_2 nanospider film grown on FTO glass (scale bars 20 and 2 μm, respectively); (c) coss-sectional SEM image of a wall edge in the nanospider thin film (scale bar 2 μm).

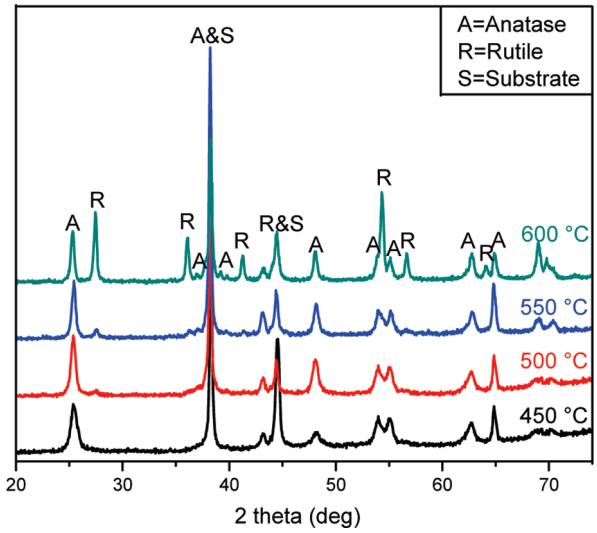

FIGURE 3. PXRD of the nanospider thin film annealed to specified temperatures (A, anatase phase; R, rutile phase; S, substrate).

accounts for the lack of any homogeneous nanospider film in the case of $Ti(O^nBu)_4$ and $Ti(O^nPr)_4$, with the presence of irregular cracks and widely varying channel width. In comparison with the nanospider morphology (Figure 1a), the formation of broader channels with higher PEG concentration (Figure 1b) can also be reasonably explained by this phase separation mechanism. It is also possible that the morphologies arise because of a drying effect.

We further investigated the effect of annealing temperature on the crystallinity, phase, and PEC performance of the TiO_2 nanospider thin film. Figure 3 presents the powder X-ray diffraction (PXRD) patterns of titania films annealed to various temperatures. As polyethylene glycol is known to decompose after 430 °C and FTO degrades (in terms of optical and transport properties) above 600 °C, annealing temperatures between 450 and 600 °C were investigated. If a TiO_2 sample is a mixture of anatase and rutile, the weight fraction of both can be calculated from eq 1 (26)

$$\text{wt \% (rutile)} = A_R/(0.884A_A + A_R) \times 100\% \quad (1)$$

where A_A represents the integrated intensity of the anatase (101) peak positioned at 25.3° and A_R is that of the rutile (110) peak located at 27.4°. There is a gradual phase transition from anatase to rutile above 500 °C. Pure anatase can be obtained only at 450 °C (weight fractions of anatase/rutile are shown in Table S1 in the Supporting Information). The crystal size of the annealed film can also be estimated by the Scherrer equation

$$\tau = 0.9\lambda/\beta\cos\theta \quad (2)$$

where τ is crystal size, λ is PXRD wavelength, β is the line broadening factor, and θ is the Bragg angle. From this calculation, the crystal size gradually increases with annealing temperature from ca. 10 to 30 nm (see Table S1 in the Supporting Information). The TEM image after 500 °C annealing shows average TiO_2 particle size ~15 nm (see Figure S2 in the Supporting Information), which agrees well with the Scherrer calculation and confirms that the films are highly nanocrystalline in nature.

A standard method to establish the efficiency of a semiconductor photocatalyst is to test the photodegradation of methylene blue (MB). This benchmark reaction requires that the catalyst have large surface area and effective dye adsorptive capability. The mechanistic details of organic photodecomposition have been discussed elsewhere (8, 27, 28), and a simplified scheme is described as follows

$$TiO_2 + \text{dye} \leftrightarrow TiO_2\text{-dye} \quad (3)$$

$$TiO_2\text{-dye} + h\nu \rightarrow TiO_2(e^-, h^+)\text{-dye} \quad (4)$$

$$TiO_2(h^+) + H_2O \rightarrow TiO_2(OH\bullet) + H^+ \quad (5)$$

$$TiO_2(h^+) + OH^- \rightarrow TiO_2(OH\bullet) \quad (6)$$

$$TiO_2(e^-) + O_2 \rightarrow TiO_2(O_2^-\bullet) \quad (7)$$

$$TiO_2(OH\bullet) + TiO_2(O_2^-\bullet) + \text{dye} \rightarrow \text{degradation products} + TiO_2 \quad (8)$$

The first dye adsorption step is the rate-determining step and prefers a large surface area TiO_2 nano/mesostructure. Photocatalytic efficiency can thus be enhanced with higher TiO_2 semiconductor-liquid contact. We employed a 1 cm × 1 cm area nanospider thin film (<0.01 g) to photodegrade 5 mL of a 1×10^{-5} M MB aqueous solution under illumination by a 6 W compact UV lamp at a fixed distance of 10 cm. Before photocatalysis, absorption/desorption equilibrium was achieved by immersing the thin film into the MB solution for 10 min under dark conditions. Our nanospider thin films are free-standing and chemically stable in the dye solution unlike commercial P25 powders. Thus, centrifuging or other particle suspension methods are not required after the catalytic reaction. During the photodegradation step, the concentration of MB solution decreased incrementally for all samples of nanospider thin films (see Figures S3 and S4 in the Supporting Information). The most efficient sample was the nanospider annealed at 500 °C, with turnover decreasing for the 550 °C annealed film. Notably, the former outperforms the P25 thin film, with more than 20% higher efficiency (Figure 4).

Photodegradation of MB has previously been shown by others to obey pseudofirst-order kinetics. Hence, the

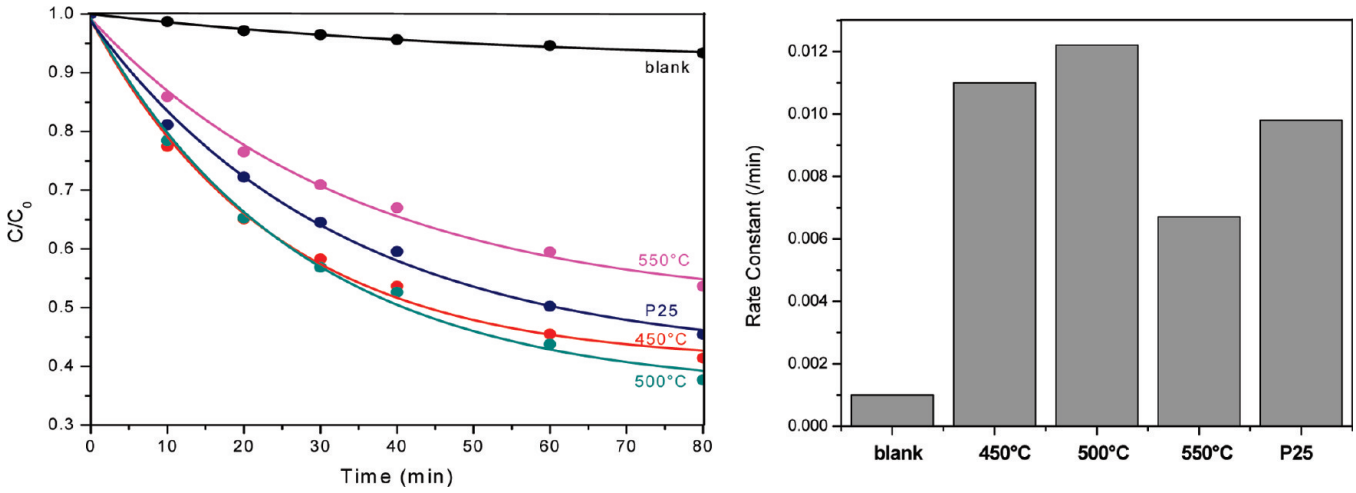

FIGURE 4. Concentration vs time plots (left) and reaction rate constants (right) for MB photolysis under UV light (blank is without UV light).

rate of MB degradation was obtained from a first-order plot (27)

$$\ln(c/c_0) = kt \tag{9}$$

where c_0 is the initial concentration of MB, c is the concentration of MB after time t of photolysis, and k is the rate constant. The highest rate constant among our nanospider samples was 0.012 min^{-1}, which is 22% higher than the commercial photocatalyst P25 film (Figure 4). The open channel system and high crystallinity of the nanospider film facilitates MB adsorption onto the spider surface, achieving higher photocatalytic efficiency with less semiconductor material.

Because of the above superior photodecomposition performance over current titania thin films, we further investigated application of the nanospider as a PEC cell for water splitting to produce hydrogen. Surface area, crystallinity, and particle size are well-known to strongly affect the photoelectrochemical properties of the semiconductor. High crystallinity reduces defects that serve as recombination trapping sites and decrease photocatalytic ability. At the same time, smaller particle size is also preferred for shorter path distance between electron−hole and surface active sites. Considering the 500 °C annealed sample had the highest MB photodegradation performance, systematic measurements were carried out on this sample, as well as a P25 thin film and a TiO_2 thin film with nanoparticle size ~15 nm for reference. All three TiO_2 samples have similar band gaps and therefore UV−vis absorption spectra (see Figure S5 in the Supporting Information). During the photoelectrochemical test, all three samples had a pronounced photocurrent beginning from approximately −0.6 V (vs Ag/AgCl), with a saturated photocurrent at −0.1 V (Figure 5a). The nanospider thin film reached 230 $\mu A/cm^2$ at 0 V and 272 $\mu A/cm^2$ at +1.1 V. In stark contrast, the P25 thin film reaches only 110 $\mu A/cm^2$ with no applied potential and 125 $\mu A/cm^2$ at +1.1 V. A thin film with particle diameter of ~15 nm (see Figure S6 in the Supporting Information) of pure anatase phase prepared by acid hydrolysis was also tested. Despite having the same particle size, the lack of nanochannels led to a much lower saturated photocurrent density of around 130 $\mu A/cm^2$, just over half that of the nanospider sample.

We also collected amperometric $I-t$ curves to study the photoresponse of the nanospider, P25, and 15 nm films; three light on/off cycles were examined. All three electrodes displayed similar low dark currents $<1 \times 10^{-7}$ A/cm^2. With illumination, however, the nanospider photocurrent is around twice than that of the P25 and 15 nm film (Figure 5b). The nanospider is also highly stable chemically and photolytically in solution under sunlight illumination, with only a very small decay with light on/off cycles. The efficiency of incident photon to chemical energy can be expressed by the following equation (28)

$$\eta = j_p(1.23 - |E_{app}|)/J_{light} \tag{10}$$

where η is the overall efficiency, j_p (A) is the photocurrent density, J_{light} (W) is the sunlight illumination intensity, and $|E_{app}|$ is the absolute value of the applied potential E_{app}, which is obtained as

$$E_{app} = E_{meas} - E_{aoc} \tag{11}$$

where E_{meas} is the electrode potential at which j_p was measured and E_{aoc} is the open circuit potential in the same electrolyte solution and illumination conditions at which j_p was measured. $E_{aoc} = -0.6$ V (vs Ag/AgCl) for nanospider, E_{aoc} for P25 is estimated to be −0.7 V, and $E_{aoc} = -0.5$ V for the 15 nm film. The small variation is due to the difference in flat band potential caused by either nanochannels, leading to less coverage of substrate or larger particle size and exposure of the substrate to electrolyte (29). With correction for optical loss in the equipment setup (25%), the TiO_2 nanospider thin film reaches 0.23% overall light-to-

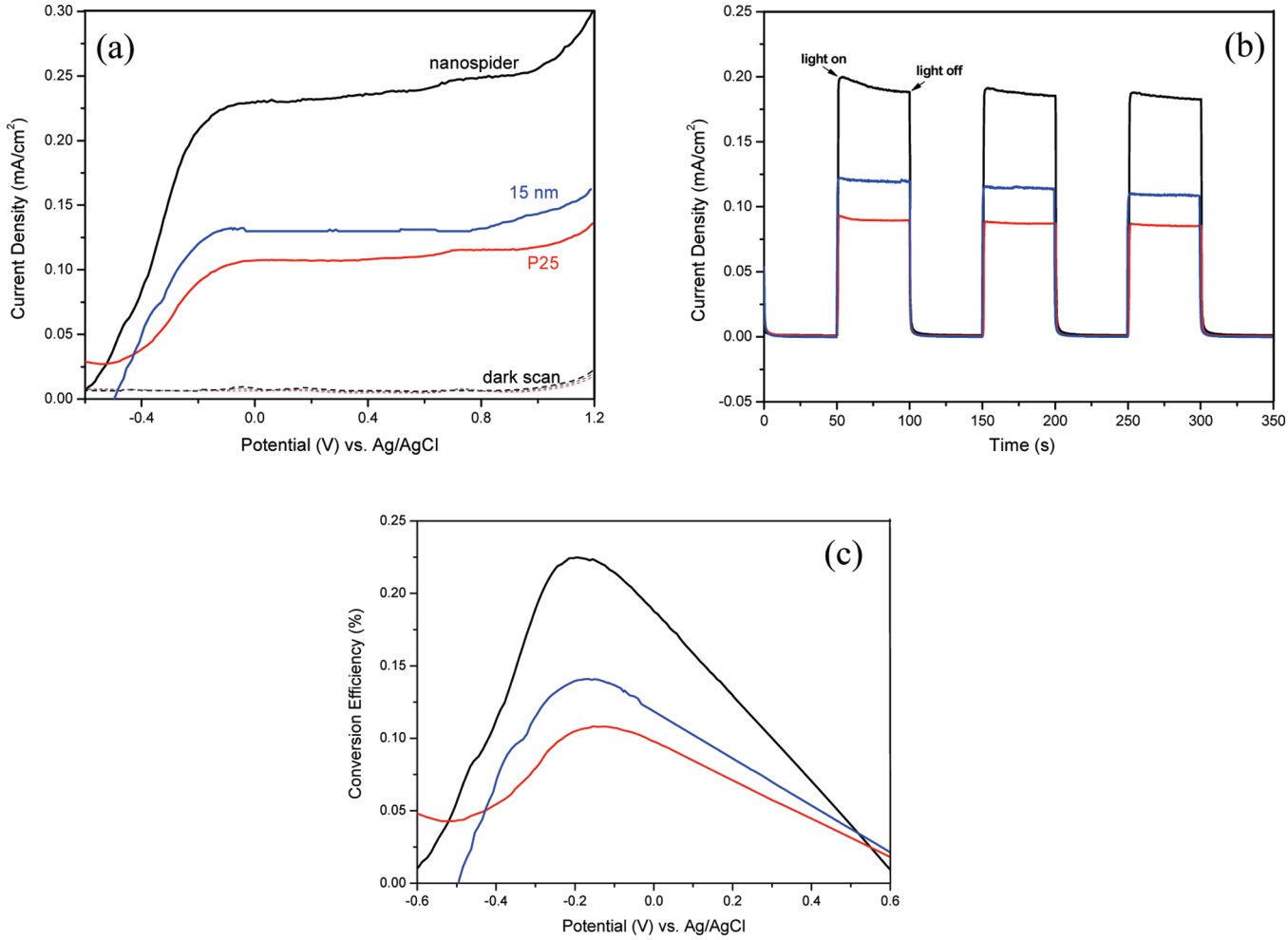

FIGURE 5. (a) Linear sweep voltammograms, collected at a scan rate of 10 mV/s from −0.6 to +1.2 V for the nanospider (black), P25 (red), and 15 nm (blue) films. Solid curves are for 100 mV/cm² illumination, whereas dark conditions are shown as dashed curves; (b) amperometric *I*−*t* curves of the nanospider (black), P25 (red), and 15 nm (blue) films at an applied voltage of +0.2 V and 100 mW/cm² illumination with 50 s light on/off cycles; (c) photoconversion efficiency of PEC cells for the nanospider (black), P25 (red) and 15 nm (blue) electrodes as a function of potential vs Ag/AgCl.

hydrogen efficiency at −0.15 V (vs Ag/AgCl) (Figure 5c). The overall efficiency of the P25 thin film is only 0.08%, and 0.11% for the 15 nm film. Although our result is less than the highest reported 0.75% achieved by a single-crystal nanowire array (12), the efficiency of the nanospider is among the highest value for a conventionally deposited TiO_2 thin film, as compared with other 0D and 1D TiO_2 nanostructures (13, 14, 29, 30). To further illustrate our nanospider PEC efficiency, we also tested a sacrificial electrolyte of Na_2S and Na_2SO_3 (see Figure S7 in the Supporting Information). In this case, the nanospider displayed a more than five times larger photocurrent than Degussa P25. This supports our conclusion that controllable nanochannels is a favorable morphology for photoelectrochemical water splitting applications.

In summary, we report a facile and low-cost method to template titania thin films with a nanospider morphology of large area and homogeneity. This material displayed both intriguing morphology and efficient application in methylene blue degradation and photoelectrochemical water splitting. The PEC photocurrent density of the nanospider working electrode was two times larger than that of the thin film with same particle size but no nanospider morphology. In future work, we aim to dope/incorporate other metal/metal oxide nanostructures into the nanochannels with controllable width throughout the film to possibly further enhance the photocatalytic efficiency.

Acknowledgment. We are grateful to Prof. Jin Z. Zhang's lab for using the PEC equipment in his lab, which is supported by the BES Division of the U.S. DOE (05ER4623A00). We thank Gongming Wang of Prof. Yat Li for photoelectrochemical measurements and Xiongwu Kang of Prof. Shaowei Chen's group for help with TEM measurements.

Supporting Information Available: Additional SEM, TEM, and optical microscope images; UV−vis spectra of TiO_2 thin films; tabulated particle size and phase weight percentage; and PXRD and TEM characterization of the 15 nm thin film (PDF). This material is available free of charge via the Internet at http://pubs.acs.org.

REFERENCES AND NOTES

(1) Oregan, B.; Gratzel, M. *Nature* **1991**, *353*, 737–740.
(2) Fujishima, A.; Honda, K. *Nature* **1972**, *238*, 37–38.
(3) Law, M.; Greene, L. E.; Johnson, J. C.; Saykally, R.; Yang, P. D. *Nat. Mater.* **2005**, *4*, 455–459.
(4) Brammer, K. S.; Oh, S. H.; Gallagher, J. O.; Jin, S. H. *Nano Lett.* **2008**, *8*, 786–793.
(5) Casavola, M.; Grillo, V.; Carlino, E.; Giannini, C.; Gozzo, F.; Pinel, E. F.; Garcia, M. A.; Manna, L.; Cingolani, R.; Cozzoli, P. D. *Nano Lett.* **2007**, *7*, 1386–1395.
(6) Pan, Y.-X.; Liu, C.-J.; Wiltoski, T. S.; Ge, Q. *Catal. Today* **2009**, *147*, 68–76.
(7) Cai, Y. Q.; Shi, Y. L.; Zhang, P.; Mou, S. F.; Jiang, G. B. *Prog. Chem.* **2006**, *18*, 1554–1564.
(8) Wu, C. H.; Chern, J. M. *Ind. Eng. Chem. Res.* **2006**, *45*, 6450–6457.
(9) Olah, G. A.; Goeppert, A.; Prakash, G. K. S. *J. Org. Chem.* **2009**, *74*, 487–498.
(10) Dai, W. L.; Luo, S. L.; Yin, S. F.; Au, C. T. *Appl. Catal., A* **2009**, *366*, 2–12.
(11) Grimes, C. A. *J. Mater. Chem.* **2007**, *17*, 1451–1457.
(12) Feng, X. J.; Shankar, K.; Varghese, O. K.; Paulose, M.; Latempa, T. J.; Grimes, C. A. *Nano Lett.* **2008**, *8*, 3781–3786.
(13) Wu, G. S.; Wang, J. P.; Thomas, D. F.; Chen, A. C. *Langmuir* **2008**, *24*, 3503–3509.
(14) Wolcott, A.; Smith, W. A.; Kuykendall, T. R.; Zhao, Y. P.; Zhang, J. Z. *Small* **2009**, *5*, 104–111.
(15) Yang, X.; Wolcottt, A.; Wang, G.; Sobo, A.; Fitzmorris, R. C.; Qian, F.; Zhang, J. Z.; Li, Y. *Nano Lett.* **2009**, *9*, 2331–2336.
(16) Ahn, K. S.; Yan, Y.; Shet, S.; Deutsch, T.; Turner, J.; Al-Jassim, M. *Appl. Phys. Lett.* **2007**, *91*, 092103.
(17) Tian, B. Z.; Liu, X. Y.; Tu, B.; Yu, C. Z.; Fan, J.; Wang, L. M.; Xie, S. H.; Stucky, G. D.; Zhao, D. Y. *Nat. Mater.* **2003**, *2*, 159–163.
(18) Yue, W. B.; Xu, X. X.; Irvine, J. T. S.; Attidekou, P. S.; Liu, C.; He, H. Y.; Zhao, D. Y.; Zhou, W. Z. *Chem. Mater.* **2009**, *21*, 2540–2546.
(19) Deshpande, A. S.; Shchukin, D. G.; Ustinovich, E.; Antonietti, M.; Caruso, R. A. *Adv. Funct. Mater.* **2005**, *15*, 239–245.
(20) Fan, X.; Fei, H.; Demaree, D. H.; Brennan, D. P.; John, J. M. S.; Oliver, S. R. J. *Langmuir* **2009**, *25*, 5835–5839.
(21) Liang, C. D.; Li, Z. J.; Dai, S. *Angew. Chem., Int. Ed.* **2008**, *47*, 3696–3717.
(22) Drisko, G. L.; Luca, V.; Sizgek, E.; Scales, N.; Caruso, R. A. *Langmuir* **2009**, *25*, 5286–5293.
(23) Fan, X. J.; Demaree, D. P.; John, J. M. S.; Tripathi, A.; Oliver, S. R. J. *Appl. Phys. Lett.* **2008**, *92*, 193108.
(24) Tran, D. T.; Fan, X. J.; Brennan, D. P.; Zavalij, P. Y.; Oliver, S. R. J. *Inorg. Chem.* **2005**, *44*, 6192–6196.
(25) Hakim, S. H.; Shanks, B. H. *Chem. Mater.* **2009**, *21*, 2027–2038.
(26) Zhang, H. Z.; Banfield, J. F. *J. Phys. Chem. B* **2000**, *104*, 3481–3487.
(27) Testino, A.; Bellobono, I. R.; Buscaglia, V.; Canevali, C.; D'Arienzo, M.; Polizzi, S.; Scotti, R.; Morazzoni, F. *J. Am. Chem. Soc.* **2007**, *129*, 3564–3575.
(28) Ryu, Y. H.; Kim, M. J.; Lee, J. D.; Yoon, C. S.; Kim, J. H.; Kim, J. H. *J. Nucl. Med.* **2002**, *43*, 347p–348p.
(29) Fabregat-Santiago, F.; Garcia-Belmonte, G.; Bisquert, J.; Bogdanoff, P.; Zaban, A. *J. Elecrochem. Soc.* **2003**, *150*, E293–E298.
(30) Oliva, F. Y.; Avalle, L. B.; Santos, E.; Camara, O. R. *J. Photochem. Photobiol. A.* **2002**, *146*, 175–188.

AM100087B